Available online at www.sciencedirect.com

ScienceDirect

journal homepage: www.elsevier.com/locate/he

Short Communication

Insight into hydrostatic pressure effects on diffusible hydrogen content in wet welding joints using in-situ X-ray imaging method

Hao Chen [a,b], *Ning Guo* [a,b,c,*], *Cheng Liu* [b], *Xin Zhang* [a,b], *Changsheng Xu* [a,b], *Guodong Wang* [a,b]

[a] *State Key Laboratory of Advanced Welding and Joining, Harbin Institute of Technology, Harbin, 150001, China*

[b] *Shandong Provincial Key Laboratory of Special Welding Technology, Harbin Institute of Technology at Weihai, Weihai, 264209, China*

[c] *Shandong Institute of Shipbuilding Technology, Weihai, 264209, China*

HIGHLIGHTS

- Gas evolution in the molten pool and droplet was imaging by in-situ X-ray method.
- High hydrostatic pressure suppressed hydrogen escaping from molten pool.
- High pressure significantly increased diffusible hydrogen content in welds.
- High hydrogen partial pressure and rapid cooling rate are the main reasons.

GRAPHICAL ABSTRACT

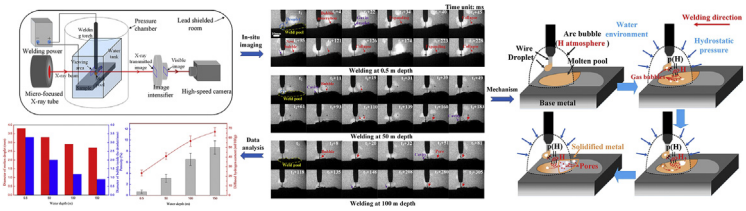

ARTICLE INFO

Article history:
Received 6 January 2020
Received in revised form
23 January 2020
Accepted 25 January 2020
Available online xxx

Keywords:
Underwater wet welding
Diffusible hydrogen

ABSTRACT

In this study, a special phenomenon of gas evolution in the metal droplet and melt pool during underwater wet welding was investigated by in-situ imaging method in a simulated deep-water environment. In general, the dissolved hydrogen escaped from molten droplet and molten pool in the form of bubbles during molten metal solidification. As the increase of hydrostatic pressure, the gas cannot expand enough to burst the droplet and release gas, but instead of entering into molten pool again. The combinations of the internal pressure in the bubble and hydrogen-rich atmosphere induced by welding arc resulted in that the melt pool has been subjected to dual influences. The diffusible hydrogen content in the deposited metal significantly increased from 23.3 to 66.3 ml/100 g with increasing the water

* *Corresponding author*. No.2 Wenhuaxi Road, Weihai, 264209, China.
E-mail address: gn21c@126.com (N. Guo).

https://doi.org/10.1016/j.ijhydene.2020.01.195

Hydrostatic pressure
X-ray imaging method

depth to 150 m, which was related to the high hydrogen partial pressure and the rapid solidification rate of molten metal.

Introduction

Deep-sea exploration is becoming a major energy resource in the future due to amounts of marine resources including oil, gas and minerals in the deep ocean [1,2]. In recent years, the continuous improvement of resources exploitation in the deep-sea promotes the wide application of underwater welding in the field of offshore steel structures such as submerged pipelines and offshore oil platforms [3–5]. Compared with dry or local cavity welding method, wet welding has the advantage of easy operability and extremely low cost [6–8]. Self-shielded flux-cored arc welding (FCAW) is promising in the future due to its better suitability for automatic welding processes conducted in deep-water than that of underwater manual metal arc welding [9–11]. However, directly contact water during welding process will have a series of adverse effects on arc ability, welding metallurgy and mechanical properties of joints [12,13]. The high level for diffusible hydrogen content in deposited metal is a serious problem in the underwater wet welding, especially at a deep-water environment [14–16]. The damaging effects of hydrogen in steels, such as hydrogen-induced cracking and hydrogen embrittlement, have been recognized as important reasons that reduce the reliability of welded structure [17–22]. Welding pores induced by hydrogen are another factor responsible for mechanical properties reduction such as toughness, ductility, yield and ultimate strength [23–25]. Spectroscopic analysis revealed that the arc plasma of the underwater wet FCAW contained the H element, providing hydrogen-enriched environments for the solidification of melt metal during welding process [26,27]. Some researchers have shown that the diffusible hydrogen content of deposited metal has obvious changes obtained in different depth of water. However, they could not reach an agreement on this issue. Ando and Asahina observed no significant changes in the diffusible hydrogen with increasing depth from 0.3 m to 20 m [28]. Silva et al. found that diffusible hydrogen content decreased from 95.3 to 60.5 ml/g significantly with increasing the water depth from 0.3 m to 30 m [29]. This discrepant result may be caused by different measurement methods for diffusible hydrogen content, diameter of the electrode and welding current. At present, low hydrogen type consumables has been produced by adding oxidizing ingredients and fluorides to the flux formulation, which can reduce the diffusible hydrogen content to below 20 ml/100 g [30–32]. But in the past, the measurements of diffusible hydrogen content often were completed by mercury method and glycerin method [33–36]. The mercury method was limited because of testing medium toxicity and the glycerin method showed a large measurement error [37,38]. It is necessary to use a more accurate measure method such as the thermal conduction gas chromatography to reveal the effects of hydrostatic pressure on the solubility and diffusivity of hydrogen in the deep-water environment.

Restricted by imaging techniques, the effect of hydrostatic pressure on diffusible hydrogen in steel during wet welding is rarely reported. And almost all of the current studies only focus on the microstructure and property of weld joint after welding. Based on the strong penetration, X-ray can overcome the reflection and refraction effects of surrounding water and traverse melt pool. Thus, X-ray transmission method can be used to observe the melt pool behaviors and metal transfer process [39–41].

In this study, it is first attempt to obtain the in-situ images of gas evolutions inside the metal melt in a deep-water environment. The results supported the conclusion that diffusible hydrogen content was increased with hydrostatic pressure.

Experimental

The underwater flux-cored wet welding was performed on the EH40 ship steel in a hyperbaric which was self-designed to simulate the deep-water hydrostatic environment. The filler material is a specially developed tubular self-shielded TiO_2-$-Fe_2O_3$ slag system low-hydrogen type flux-cored wire with a diameter of 1.6 mm. The sheath material of flux-cored wire was a low-carbon steel strip of H08A. The chemical composition of EH40 and H08A steel are shown in Table 1. Some mineral powders such as Fe_2O_3 and CaF_2 were added in the flux-core to reduce the hydrogen dissolved in weld metal. Welding with DCEP polarity was conducted in a water tank filled with water of 0.5 m depth. Above the water, the air in chamber was pressurized to 0.5, 1.0 and 1.5 MPa to simulate the hydrostatic pressure environment of depth of 50, 100 and 150 m, respectively. The welding parameters were used are listed as follows: welding voltage of 45 V, wire feed speed of 6 m/min, workpiece traveling speed of 3 mm/s, contact tip to work distance (CTWD) of 20 mm and wire extension of 15 mm. As shown in Fig. 1, the X-ray energy could penetrate the chamber, water tank, melt pool and then formed X-ray images on an image intensifier. The image intensifier converted the X-ray transmitted image to the visible continuous photographs imaged onto a computer screen by a high-speed camera (Optronis CR series). Based on the different contrasts, image

Table 1 – Chemical composition of EH40 and H08A (wt%).

Material	C	Mn	Ni	Cr	Si	P	S	Fe
EH40	0.17	1.36	0.05	0.02	0.45	0.006	0.3	Bal.
H08A	0.10	0.41	0.01	0.01	0.05	0.035	0.025	Bal.

Please cite this article as: Chen H et al., Insight into hydrostatic pressure effects on diffusible hydrogen content in wet welding joints using in-situ X-ray imaging method, International Journal of Hydrogen Energy, https://doi.org/10.1016/j.ijhydene.2020.01.195

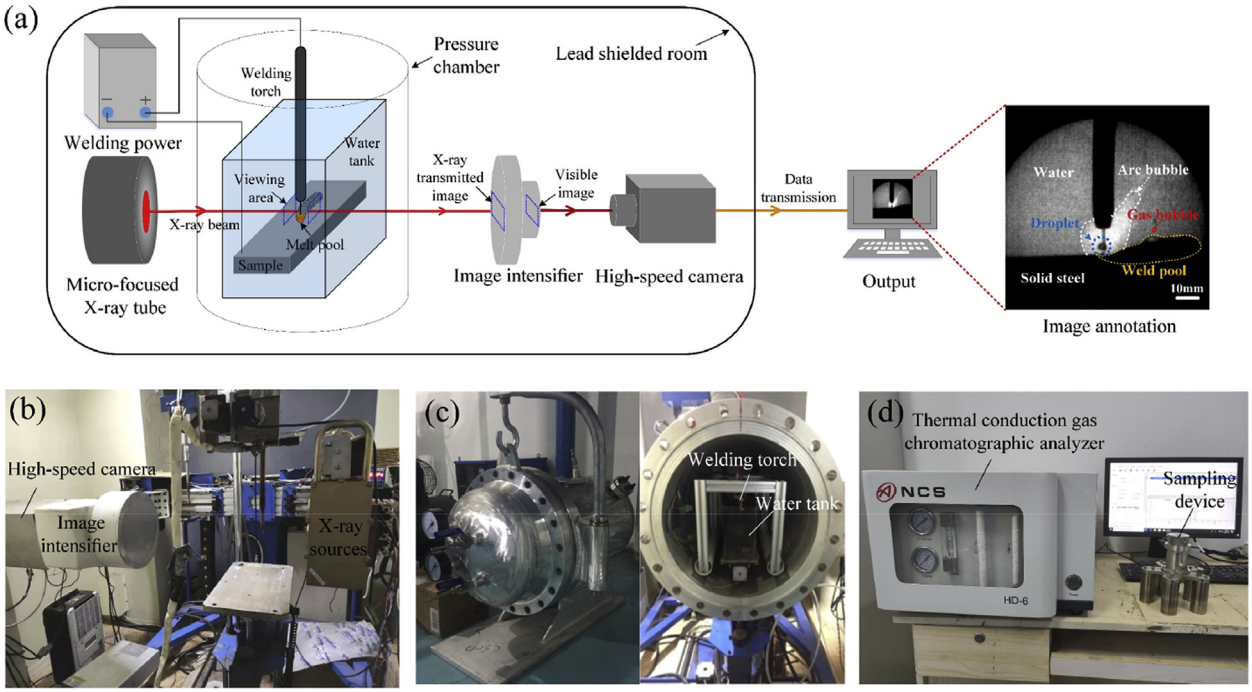

Fig. 1 – (a) Schematic diagram of the experimental setup and an example X-ray image. (b) experimental platform, (c) hyperbaric chamber internal device, (d) thermal conduction gas chromatographic analyzer.

characteristics such as melt, gas bubble and arc bubble can be distinguished. In order to ensure X-ray radiolucency and high definition images, the image parameters with 256 × 256 pixels chip and frame rate of 1000 fps were used.

The porosity of deposited metal was quantitated and calculated by the Archimedean principle according to Eq (1) [42,43].

$$\delta = \left(1 - \frac{\rho_1}{\rho_0}\right) \times 100\% \quad (1)$$

where δ is the porosity, ρ_0 is the actual density of deposited metal, ρ_1 is the apparent density of measured deposited metal.

The diffusible hydrogen content in deposited metal was determined according to the thermal conduction gas chromatographic analyzer (HD-6 provided by NCS Testing Technology CO., LTD). At least four specimens were examined in the determination experiments of porosity and diffusible hydrogen content for each set of experiments. The deposited metal and the heat-affected zone were etched with a 4% (vol%) nitric acid ethanol solution. The microstructures were observed using an OLYMPUS GX51 optical digital microscope.

Results and discussion

Gas evolution in the molten pool

Fig. 2 shows a series of images for the welding process under different hydrostatic pressures which corresponding to 0.5 m, 50 m and 100 m depth, respectively. As shown in Fig. 2(a), the sequential radiographs give the droplet transfer and melt pool dynamic process when the welding process was performed at 0.5 m depth (see details in Supplementary Movie 1). It could be obviously seen that the gas dissolved in melt pool formed a gas bubble (at t1+4 ms), then expanded (at t1+34 ms) and collapsed (at t1+45 ms). Then, a new life cycle of gas bubble began from t1+95 to t1+126 ms and from t1+174 to t1+228 ms. It could be deduced that the of gas dissolved out due to the reduced solubility caused by melt cooling. The gas bubbles took less than 50 ms from generating to collapsing. There were about 10 gas bubbles escaping from weld pool in every second and the frequency of gas evolution was relatively stable. Furthermore, it could be observed that there were some gases that escaped from molten droplet and then made a hollow droplet (at t1+22 ms). If the internal pressure of gases was high enough, the droplet would be burst and released the gases before it entered into weld pool (at t1+45). Of course, this was a periodic process throughout the lifetime of droplet. It can be found that the droplet became hollow (at t1+95 ms) and then released the excess gases again (at t1+121 ms).

Supplementary video related to this article can be found at https://doi.org/10.1016/j.ijhydene.2020.01.195.

When carried out the welding at the depth of 50 m, some different phenomena were discovered, as shown in Fig. 2(b) (see details in Supplementary Movie 2). First, the gas dissolved in melt pool could still from bubble and try to escape from melt pool. However, these bubbles gathered on the surface of the melt pool, instead of escaping from it. It is found there was very little evidence of bubble collapse throughout the process, as shown in Fig. 2(b). One of the main reasons may be that increased water pressure limited the free expansion of gas bubble, which resulted in these bubbles cannot burst and release the gas dissolved in melt pool. Second, there was cavity existing inside the front of weld pool (at t2+11 and t2+183 ms). These gases which couldn't escape in time

Please cite this article as: Chen H et al., Insight into hydrostatic pressure effects on diffusible hydrogen content in wet welding joints using in-situ X-ray imaging method, International Journal of Hydrogen Energy, https://doi.org/10.1016/j.ijhydene.2020.01.195

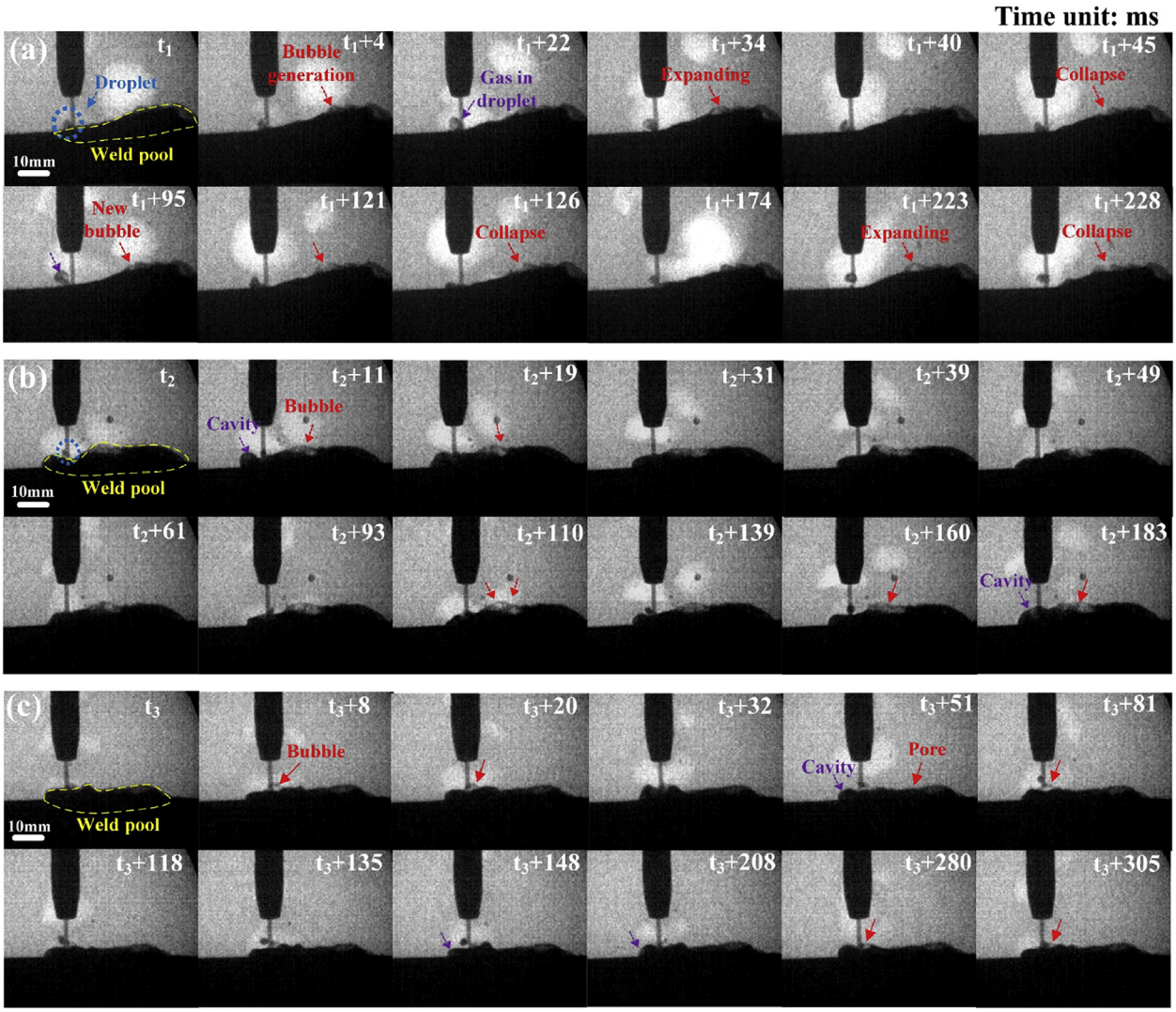

Fig. 2 – Images of welding process at different simulated depth. (a) 0.5 m, (b) 50 m and (c) 100 m.

changed the shape of the weld pool. Compared with the melt pool obtained in shallow water, the weld pool became flat with the increase of water depth. Some molten metals accumulated under the welding wire even located at the front of weld pool. There were some cavities existing in the molten metal due to the gas evolution (at t2+11 ms). Besides, the size of molten droplet decreased significantly when the water depth increased to 50 m. It was difficult to observe the gas escaping phenomenon in the droplet at this moment.

Supplementary video related to this article can be found at https://doi.org/10.1016/j.ijhydene.2020.01.195.

As the water depth further increased to 100 m, the phenomenal characters of weld pool and droplet were more obviously. As shown in Fig. 2(c), the shape of weld pool became flatter with some visible pores existing in the weld metal. The gas bubbles caused by gas escaping generated and continued to exist from t3+8 to t3+305 ms (see details in Supplementary Movie 3). In fact, some of gas bubbles kept growing, but cannot be burst due to the high hydrostatic pressure throughout the solidification of weld pool. So, these gases cannot be released and form the visible pores remained in the weld metal (at t3+51 ms). More cavities could be observed in the interior of molten metal accumulated under the welding wire.

Supplementary video related to this article can be found at https://doi.org/10.1016/j.ijhydene.2020.01.195.

Gas escaping phenomenon in the droplet

In order to study the gas escaping phenomenon in the droplet, the maximum mean diameters of molten droplet and gas bubble inside the droplet were counted, as shown in Fig. 3(a). When the welding was performed at a shallow water such as 0.5 m, the maximum diameters of droplet and bubble were 3.8 mm and 3.2 mm, respectively. With the water depth increased to 50 mm, the maximum diameter of droplet decreased to 3.3 mm and the bubble diameter decreased to 2 mm. Compared with molten droplet size, the bubble inside

Please cite this article as: Chen H et al., Insight into hydrostatic pressure effects on diffusible hydrogen content in wet welding joints using in-situ X-ray imaging method, International Journal of Hydrogen Energy, https://doi.org/10.1016/j.ijhydene.2020.01.195

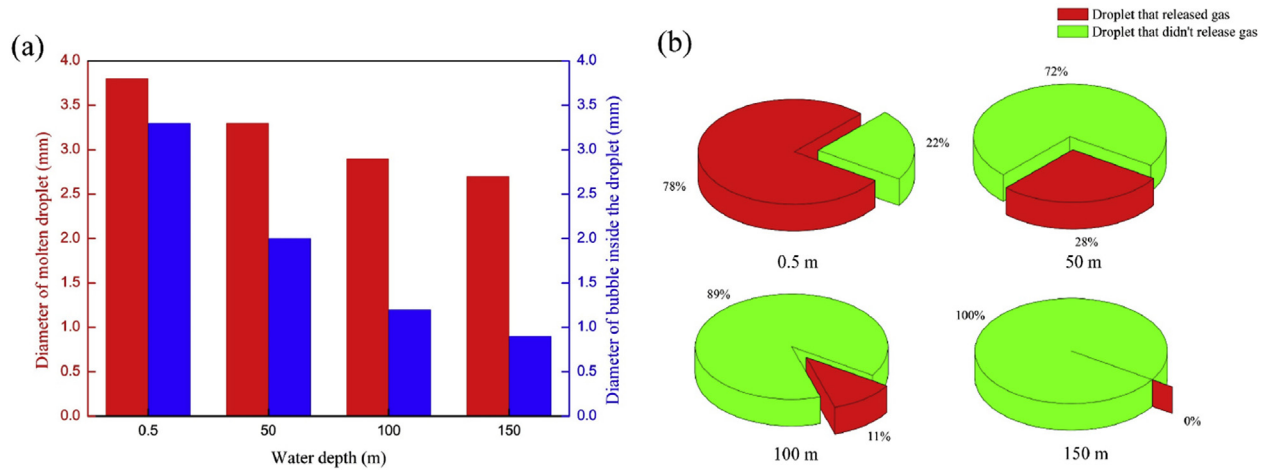

Fig. 3 – (a) Maximum mean diameters of molten droplet and gas bubble inside the droplet at different water depth. (b) Proportion of molten droplet which released gas during a whole welding process at different water depth.

the droplet showed a greater decrease in size. When the water depth was 150 m, the diameter of gas bubble was only about 0.9 mm. Some of these gas bubbles were so small that they couldn't be observed and counted in the images obtained by X-ray transmission method. This changing of bubble size with the water depth could be explained by the Boyle's law:

$$P_1V_1 = P_2V_2 \quad (2)$$

where the P_1 and the V_1 are respectively the hydrostatic pressure and bubble maximum size at shallow water (such as 0.5 m depth), the P_2 and the V_2 are respectively the hydrostatic pressure and bubble maximum size at simulated deep water (such as 150 m depth).

Actually, the amount of the released gas caused by dissolved hydrogen in the droplet and the temperature of droplet would be changed during the welding process, which resulted in the deviation between the measured value and calculated value of the bubble size at different hydrostatic pressure. The significant difference in the size of molten droplet and gas bubble meant that it was difficult for the bubble to break the droplet and release gas. Fig. 3(b) shows the proportion of molten droplet from which gas can escape during a whole welding process at different water depth. It can be seen that the proportion of gas escaping from droplet significantly decreased with the increase of water depth. When the depth was 150 m (corresponds to hydrostatic pressure of 1.5 Mpa), the proportion of the molten droplet which released gas was almost 0%. This result suggests that there was no hydrogen dissolved in the droplet could be vented in the form of gas. Amounts of hydrogen would enter into the molten pool during droplet transfer process. For molten pool, the higher pressure in deeper water provided an environment which was richer in hydrogen.

Hydrostatic pressure effect on diffusible hydrogen content

Fig. 4(a) shows the diffusible hydrogen content and porosity of weld metal obtained at water of 0.5, 50, 100 and 150 m depth, respectively. Obviously, both of them show the rising trends as the water depth increased. The porosity of weld metal increased from 0.67% to 8.67% with the water depth increased to 150 m. At 0.5 m water depth, the diffusible hydrogen content in the weld metal was 23.3 ml/100 g. As the water depth increased to 150 m, the value of diffusible hydrogen almost doubled to 66.3 ml/100 g. In general, this value of diffusible hydrogen in the weld metal is below 15 ml/100 g when the welding is carried out in an air environment using the same type of welding material. Clearly, the decomposition of the water induced a hydrogen-rich environment surrounding the welding zone, which was a major reason for the increase of diffusible hydrogen. In the deep-water environment, high hydrostatic pressure suppressed the escaping of hydrogen in the form of gas. A large amount of hydrogen gas bubbles has been left in the molten pool, and then some hydrogen gas pores were formed after the cooling of weld metal. It is well known that high hydrostatic pressure also increases hydrogen partial pressure, which increases significantly the solubility of hydrogen in the molten pool according to Eq. (3) [44].

$$S(H_2) = K(H_2)\sqrt{p(H_2)} \quad (3)$$

where $K(H_2)$ is the equilibrium constant of the H_2 dissolution reaction, depending on the temperature, $p(H_2)$ is the partial pressure of H_2 in the gas phase.

In addition, arc burning would split many H molecules into H atoms, and the solubility of this part of H can be calculated as shown in Eq. (4):

$$S(H) = K(H)p(H) \quad (4)$$

In this equation, the solubility of hydrogen is proportional to p(H) in Eq. (4) instead of $\sqrt{p(H_2)}$, which means more hydrogen dissolving into molten pool caused by high hydrostatic pressure in the deep-water. Even if calculating only by Eq. (3), the hydrogen solubility at 100 m is also three times that at a depth of 0.5 m. It is well known that the solubility of hydrogen in the liquid steel will decrease with the temperature decreasing. So that, the supersaturated hydrogen was precipitated in the form of gas bubbles during the cooling of molten pool. However, the cooling rate of molten pool was

Please cite this article as: Chen H et al., Insight into hydrostatic pressure effects on diffusible hydrogen content in wet welding joints using in-situ X-ray imaging method, International Journal of Hydrogen Energy, https://doi.org/10.1016/j.ijhydene.2020.01.195

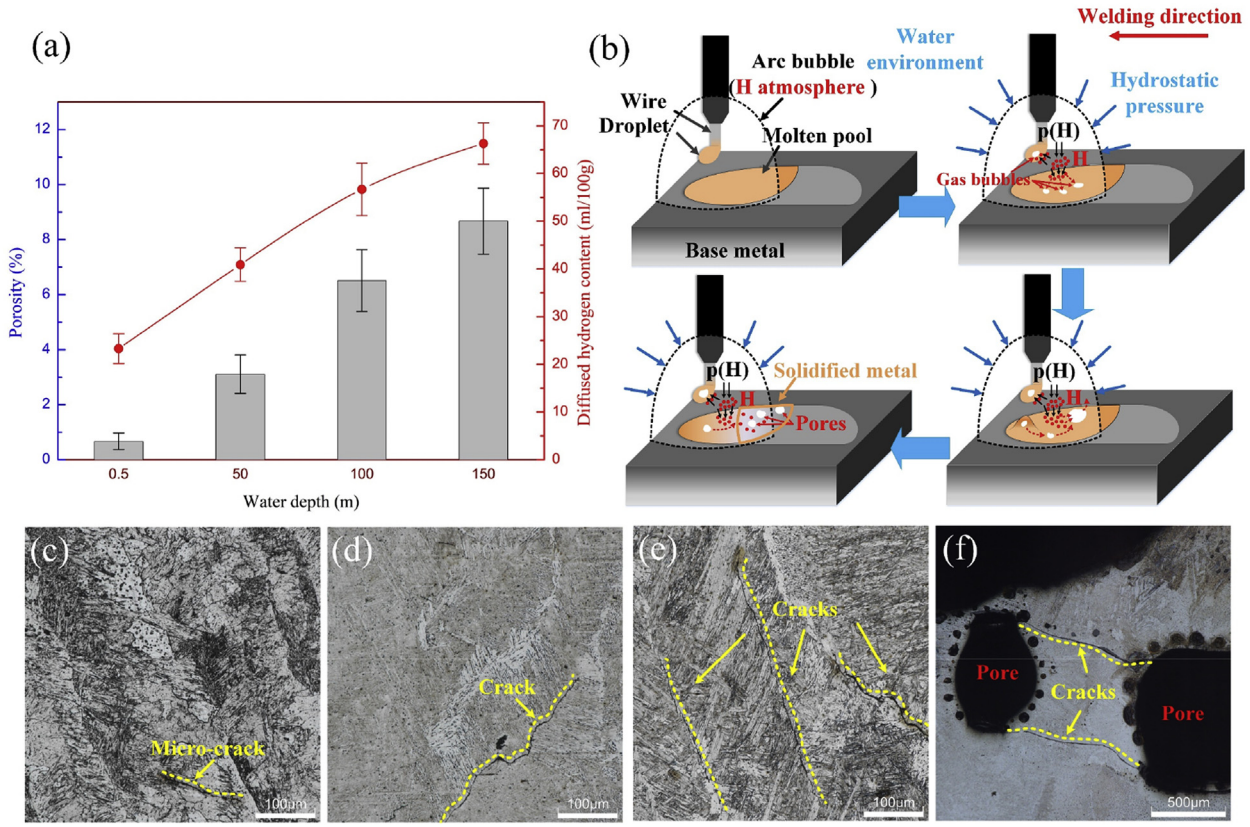

Fig. 4 – (a) The variation trend of diffusible hydrogen content and porosity in weld metal with water depth. (b) The illustration of the increase in diffusible hydrogen and pores at deep-water. Crack morphology and propagation in weld metal obtained at 50 m (c), 100 m (d) and 150 m (e, f).

extremely fast due to the he forced cooling effect of water environment. Some studies have proved that molten pool can be cooled and solidified within 10 s [39]. At this stage, not all of the dissolved hydrogen could escape from the pool in time. Bubbles that didn't escape from molten pool become hydrogen pores and remained in the weld metal, while the rest of supersaturated hydrogen would continue to diffuse and escape after welding and become diffused hydrogen. This process is shown in the Fig. 4(b).

For the welding process in a deep-water environment, the dissolved hydrogen content was much higher, while the cooling rate of the molten pool was still very fast. This result led to a significant increase in the diffusible hydrogen content in the welded joint obtained in the deep-water environment. As shown in Fig. 4(c)–(e), the mechanical properties of the weld would be greatly deteriorated, and the resulting micro-cracks were often hidden dangers of joint failure. Fig. 4(f) also shows the propagation of macro-cracks caused by the high internal stress inside the pores.

Conclusion

In summary, the effect of hydrostatic pressure on diffusible hydrogen content was investigated by in-situ X-ray imaging method. The welded joint obtained in underwater wet welding showed a high level of diffusible hydrogen content and porosity. High partial pressure of hydrogen and rapid cooling rate of molten pool were the two main reasons which resulted in the significant increase in diffusible hydrogen content and porosity in the weld metal at a deep-water environment.

Acknowledgements

The authors are grateful for the financial support for this study from the Fundamental Research Funds for the Central Universities(Grant No.HIT.NSRIF.201602, HIT.NSRIF.201704, HIT.MKSTISP.201617), the Shan dong Provincial Key Research and Development Plan (2017CXGC0922, 2018GGX103003) and Natural Science Foundation of Shandong Province (Grant No. ZR2017QEE005, ZR2017PEE010).

REFERENCES

[1] Yang ZX, Kan B, Li JX, Su YJ, Qiao LJ. Hydrostatic pressure effects on stress corrosion cracking of X70 pipeline steel in a simulated deep-sea environment. Int J Hydrogen Energy 2017;42(44):27446–57.
[2] Traverso P, Canepa E. A review of studies on corrosion of metals and alloys in deep-sea environment. Ocean Eng 2014;87:10–5.

Please cite this article as: Chen H et al., Insight into hydrostatic pressure effects on diffusible hydrogen content in wet welding joints using in-situ X-ray imaging method, International Journal of Hydrogen Energy, https://doi.org/10.1016/j.ijhydene.2020.01.195

[3] Li H, Liu D, Ma Q, Guo N, Song X, Feng J. Microstructure and mechanical properties of dissimilar welds between 16Mn and 304L in underwater wet welding. Sci Technol Weld Join 2018:1–7.
[4] Rogalski G, Fydrych D, Łabanowski J. Underwater wet repair welding of API 5L X65M pipeline steel. Pol Marit Res 2017;24(s1):188–94.
[5] Chen H, Guo N, Huang L, Zhang X, Feng J, Wang G. Effects of arc bubble behaviors and characteristics on droplet transfer in underwater wet welding using in-situ imaging method. Mater Des 2019;170:107696.
[6] Guo N, Zhang X, Xu C, Chen H, Fu Y, Cheng Q. Effect of parameters change on the weld appearance in stainless steel underwater wet welding with flux-cored wire. Metals 2019;9(9):951.
[7] Wang J, Sun Q, Ma J, Jin P, Sun T, Feng J. Correlation between wire feed speed and external mechanical constraint for enhanced process stability in underwater wet flux-cored arc welding. Proc IME B J Eng Manufact 2018:2073596762.
[8] Tomków J, Rogalski G, Fydrych D, Łabanowski J. Advantages of the application of the temper bead welding technique during wet welding. Materials 2019;12(6):915.
[9] Feng J, Wang J, Sun Q, Zhao H, Wu L, Xu P. Investigation on dynamic behaviors of bubble evolution in underwater wet flux-cored arc welding. J Manuf Process 2017;28:156–67.
[10] Guo N, Du Y, Feng J, Guo W, Deng Z. Study of underwater wet welding stability using an X-ray transmission method. J Mater Process Technol 2015;225:133–8.
[11] Guo N, Du Y, Maksimov S, Feng J, Yin Z, Krazhanovskyi D, Fu Y. Study of metal transfer control in underwater wet FCAW using pulsed wire feed method. Weld World 2018;62(1):87–94.
[12] Wang J, Sun Q, Hou S, Zhang T, Jin P, Feng J. Dynamic control of current and voltage waveforms and droplet transfer for ultrasonic-wave-assisted underwater wet welding. Mater Des 2019;181:108051.
[13] Chen H, Guo N, Shi X, Du Y, Feng J, Wang G. Effect of water flow on the arc stability and metal transfer in underwater flux-cored wet welding. J Manuf Process 2018;31:103–15.
[14] Świerczyńska A, Fydrych D, Rogalski G. Diffusible hydrogen management in underwater wet self-shielded flux cored arc welding. Int J Hydrogen Energy 2017;42(38):24532–40.
[15] Fydrych D, Swierczynska A, Rogalski G. Effect of underwater wet welding conditions on the diffusible hydrogen content in deposited metal. Metall Ital 2015;107(11–12):47–52.
[16] Padilla E, Chawla N, Silva LF, Dos Santos VR, Paciornik S. Image analysis of cracks in the weld metal of a wet welded steel joint by three dimensional (3D) X-ray microtomography. Mater Char 2013;83:139–44.
[17] Saini N, Pandey C, Mahapatra MM. Effect of diffusible hydrogen content on embrittlement of P92 steel. Int J Hydrogen Energy 2017;42(27):17328–38.
[18] Koyama M, Akiyama E, Lee Y, Raabe D, Tsuzaki K. Overview of hydrogen embrittlement in high-Mn steels. Int J Hydrogen Energy 2017;42(17):12706–23.
[19] Lu X, Ma Y, Zamanzade M, Deng Y, Wang D, Bleck W, Song WW, Barnoush A. Insight into hydrogen effect on a duplex medium-Mn steel revealed by in-situ nanoindentation test. Int J Hydrogen Energy 2019;44(36):20545–51.
[20] Laureys A, Depover T, Petrov R, Verbeken K. Characterization of hydrogen induced cracking in TRIP-assisted steels. Int J Hydrogen Energy 2015;40(47):16901–12.
[21] Singh V, Singh R, Arora KS, Mahajan DK. Hydrogen induced blister cracking and mechanical failure in X65 pipeline steels. Int J Hydrogen Energy 2019;44(39):22039–49.
[22] Pandey C, Saini N, Mahapatra MM, Kumar P. Hydrogen induced cold cracking of creep resistant ferritic P91 steel for different diffusible hydrogen levels in deposited metal. Int J Hydrogen Energy 2016;41(39):17695–712.
[23] Silva LF, Dos Santos VR, Paciornik S, Mertens JCE, Chawla N. Multiscale 3D characterization of discontinuities in underwater wet welds. Mater Char 2015;107:358–66.
[24] Pessoa ECP, Bracarense AQ, Zica EM, Liu S, Perez-Guerrero F. Porosity variation along multipass underwater wet welds and its influence on mechanical properties. J Mater Process Technol 2006;179(1):239–43.
[25] Gao W, Wang D, Cheng F, Deng C, Xu W. Underwater wet welding for HSLA steels: chemical composition, defects, microstructures, and mechanical properties. Acta Metall Sin 2015;28(9):1097–108.
[26] Jia C, Zhang T, Maksimov SY, Yuan X. Spectroscopic analysis of the arc plasma of underwater wet flux-cored arc welding. J Mater Process Technol 2013;213(8):1370–7.
[27] Jia C, Zhang Y, Zhao B, Hu JK, Wu CS. Visual sensing of the physical process during underwater wet FCAW. Weld J 2016;95(6):202–9.
[28] Ando S, Asahina T. A study on the metallurgical properties of steel welds with underwater gravity welding, underwater welding. Trondeheim: IIW Conference Pergamun Press; 1983. p. 255–61.
[29] Da Silva WCD, Bracarense AQ, Pessoa ECP. Efeito da profundidade de soldagem no hidrogenio difusivel de soldas molhadas. Soldagem e Inspecao 2012;17(4):298–305.
[30] du Plessis J, du Toit M. Reducing diffusible hydrogen contents of shielded metal arc welds through addition of flux-oxidizing ingredients. J Mater Eng Perform 2008;17(1):50–6.
[31] Rowe M, Liu S. Recent developments in underwater wet welding. Sci Technol Weld Join 2001;6(6):387–96.
[32] Matsushita M, Liu S. Hydrogen control in steel weld metal by means of fluoride additions in welding flux. Weld J 2000;79(10):295–303.
[33] Padhy GK, Ramasubbu V, Parvathavarthini N, Wu CS, Albert SK. Influence of temperature and alloying on the apparent diffusivity of hydrogen in high strength steel. Int J Hydrogen Energy 2015;40(20):6714–25.
[34] Padhy GK, Ramasubbu V, Murugesan N, Ramesh C, Parvathavarthini N, Albert SK. Determination of apparent diffusivity of hydrogen in 9Cr-1MoVNbN steel using hot extraction-PEMHS technique. Int J Hydrogen Energy 2013;38(25):10683–93.
[35] Kong X, Li C, Zou Y, Zhang J, Hu Y, Wang J. Measurement and analysis of the diffusible hydrogen in underwater wet welding joint. MATEC Web of Conferences 2016;39:3004.
[36] Fydrych D, Łabanowski J. An experimental study of high-hydrogen welding processes. Rev Metal Madrid 2015;51(4):1–7.
[37] Padhy GK, Ramasubbu V, Albert SK. Rapid determination of diffusible hydrogen in steel welds using a modified gas chromatography facility. J Test Eval 2014;43(1):69–79.
[38] Lopez FA, Sierra MJ, Rodrı´guez O, Millan R, Alguacil FJ. Nonisothermal kinetics of the thermal desorption of mercury from a contaminated soil. Rev Metal (Madr) 2014;50(1):1–10.
[39] Xu C, Guo N, Zhang X, Jiang H, Chen H, Feng J. In situ X-ray imaging of melt pool dynamics in underwater arc welding. Mater Des 2019;179:107899.
[40] Chen H, Guo N, Shi X, Du Y, Feng J, Wang G. Effect of hydrostatic pressure on protective bubble characteristic and weld quality in underwater flux-cored wire wet welding. J Mater Process Technol 2018;259:159–68.

Please cite this article as: Chen H et al., Insight into hydrostatic pressure effects on diffusible hydrogen content in wet welding joints using in-situ X-ray imaging method, International Journal of Hydrogen Energy, https://doi.org/10.1016/j.ijhydene.2020.01.195

[41] Leung CLA, Marussi S, Towrie M, Atwood RC, Withers PJ, Lee PD. The effect of powder oxidation on defect formation in laser additive manufacturing. Acta Mater 2019;166:294–305.
[42] Xie B, Zhao H, Long H, Peng J, Liu R. 3D characteristics of pores in SiC particle preforms with different starch contents by X-ray micro-computed tomography. Ceram Int 2019;45(18):23924–33.
[43] Chen H, Guo N, Xu K, Xu C, Zhou L, Wang G. In-situ observations of melt degassing and hydrogen removal enhanced by ultrasonics in underwater wet welding. Mater Des 2020;188:108482.
[44] Liu H. Welding metallurgy and weldability. Beijing: China Machine Press; 2007. p. 52–4.

Please cite this article as: Chen H et al., Insight into hydrostatic pressure effects on diffusible hydrogen content in wet welding joints using in-situ X-ray imaging method, International Journal of Hydrogen Energy, https://doi.org/10.1016/j.ijhydene.2020.01.195